Lab on a Chip

Accepted Manuscript

ROYAL SOCIETY OF CHEMISTRY

www.rsc.org/loc

Advanced LSI-based amperometric sensor array with light-shielding structure for effective removal of photocurrent and mode selectable function for individual operation of 400 electrodes

Kumi Y. Inoue,[*ab] Masahki Matsudaira,[b] Masanori Nakano,[a] Kosuke Ino,[a] Chika Sakamoto,[a] Yusuke Kanno,[a] Reyushi Kubo,[a] Ryota Kunikata,[c] Atsushi Kira,[c] Atsushi Suda,[c] Ryota Tsurumi,[d] Toshihito Shioya,[d] Shinya Yoshida,[f] Masanori Muroyama,[be] Tomohiro Ishikawa,[be] Hitoshi Shiku,[abf] Shiro Satoh,[b] Masayoshi Esashi,[bf] and Tomokazu Matsue[*abf]

[a]*Graduate School of Environmental Studies, Tohoku University, 6-6-11 Aramaki-Aza-Aoba, Aoba-ku, Sendai 980-8579, Japan*
[b]*Micro System Integration Center (μSIC), Tohoku University, 519-1176 Aramaki-Aza-Aoba, Aoba-ku, Sendai 980-0845, Japan*
[c]*Japan Aviation Electronics Industry, Limited, 1-21-2 Dogenzaka, Shibuya-ku, Tokyo 150-0043, Japan*
[d]*Toppan Technical Design Center Co., Ltd., 1-5-1, Taito, Taito-ku, Tokyo 110-0016, Japan*
[e]*Graduate School of Engineering, Tohoku University, 6-6-01 Aramaki-Aza-Aoba, Aoba-ku, Sendai 980-8579, Japan*
[f]*The World Premier International Research Center Advanced Institute for Materials Research (WPI-AIMR), Tohoku University, 2-1-1 Katahira, Aoba-ku, Sendai 980-8579, Japan*

*Corresponding authors:

Kumi Inoue, Graduate School of Environmental Studies, Tohoku University, 6-6-11 Aramaki-Aza-Aoba, Aoba-ku, Sendai 980-8579, Japan
Tel: +81-22-795-6167
Fax: +81-22-795-6167
E-mail: inoue@bioinfo.che.tohoku.ac.jp

Tomokazu Matsue, The World Premier International Research Center Advanced Institute for Materials Research (WPI-AIMR), Tohoku University, 2-1-1 Katahira, Aoba, Sendai 980-8579, Japan
Tel: +81-22-795-7281
Fax: +81-22-795-7281
E-mail: matsue@bioinfo.che.tohoku.ac.jp

ABSTRACT

We have developed a large-scale integrated (LSI) complementary metal-oxide semiconductor (CMOS)-based amperometric sensor array system called "Bio-LSI" as a platform for electrochemical bio-imaging and multi-point biosensing with 400 measurement points. In this study, we newly developed a Bio-LSI chip with light-shield structure and mode-selectable function with the aim to extend the application range of Bio-LSI. The light shield created by the top metal layer of the LSI chip significantly reduces the noise generated by the photocurrent, whose value is less than 1% of the previous Bio-LSI without the light shield. The mode-selectable function enables the individual operation of 400 electrodes in off, electrometer, V1, and V2 mode. The off-mode cut the electrode from the electric circuit. The electrometer-mode read out the electrode potential. The V1-mode and the V2-mode set the selected sensor electrode at two different independent voltages and read out the current. We demonstrated the usefulness of the mode-selectable function. First, we displayed a dot picture based on the redox reactions of 2.0 mM ferrocenemethanol at 400 electrodes applied two different independent voltages using V1 and V2 mode. Second, we carried out using the V1 and V2 modes. Third, we used the off and V1 modes for the modification of the osmium-polyvinylpyridine gel polymer containing horseradish peroxidase (Os-HRP) at the selected electrodes, which act as sensors for H_2O_2.These results confirm that the

advanced version of Bio-LSI is a promising tool that can be applied to a wide range of analytical fields.

KEYWORDS: Active pixel sensor, Amperometric sensor, Analog circuit, Bioimaging, Biosensor, Complementary metal-oxide semiconductor (CMOS), Electrode array, Integrated potentiostat

1. Introduction

The large integration of electrochemical sensors into a small chip is a promising technology for rapid and high-throughput chemical analysis as well as for bioimaging using each sensor as an image pixel. Potentiometric sensor arrays that are mainly based on field-effect transistors (FETs) have been extensively used for label-free DNA sensing, dynamic imaging of the extracellular activities of neuronal networks, and for other sensors for biological assays.[1-3] In contrast, studies using amperometric sensor arrays[4-9] with over 100 detection points are limited because the integration of high-performance potentiostat circuits is difficult compared to that of FETs for potentiometric sensors. Amperometry is a widely employed electrochemical technique for bio/chemical sensors including the commercially produced glucose sensors for diabetes, because amperometry provides direct information about the concentration of the analyte as a redox current. The integration of large numbers of amperometric sensors on a single chip is greatly desired for the rapid and high-throughput quantitative analysis of biomolecules and bioimaging.

We have previously developed a large-scale integrated (LSI) complementary metal-oxide semiconductor (CMOS)-based amperometric sensor called “Bio-LSI” with 400 measurement points as a platform for electrochemical bioimaging and multi-point

biosensing.[10] We successfully realized a wide dynamic range from ±1 pA to ±100 nA using a well-designed circuit and operating software with switched-capacitor I-V conversion. The spatial resolution of Bio-LSI is 250 μm. The temporal resolution varies from 18 ms/image to 125 ms/image according to the selection of the current measuring range. We call this first version of Bio-LSI "1G Bio-LSI." Using 1G Bio-LSI, we successfully acquired images of the activity of glucose oxidase,[10,11] as well as an undifferentiated marker (alkaline phosphatase activity[12,13] and sarcomeric a-actinin[13]) of embryoid bodies consisting of living cells and gene silencing. However, the CMOS based sensor system has a weak point of generation of a photocurrent noise under the light irradiation. In the previous paper[10], we suppressed over 70 % of the photocurrent by covering the surface of the LSI chip with Au sputtered film but still over 20 pA was observed under the most intense lighting condition of a microscope. It is a serious obstacle for the biosensing requiring higher sensitivity. We also considered that minor changes of the LSI circuit would significantly increase the freedom of measurements and operations of the Bio-LSI. With 1G Bio-LSI, all 400 sensing point are under same operation, which limits the application of Bio-LSI.

In this paper, we present a newly developed advanced version of Bio-LSI called "2G Bio-LSI" which has the same outward appearance as 1G Bio-LSI with 250-μm-pitched

400 measurement points at the center area of a 10.4 mm × 10.4 mm CMOS sensor chip (Figure 1). Advanced points of the 2G Bio-LSI are an effective removal of photocurrent noise and an improvement of control/measurement circuit to allow individual operation of 400 electrodes. The light shield created by the top metal layer of the LSI chip significantly reduces the noise generated by the photocurrent. The noise level of the 2G Bio-LSI is less than 1% of the 1G Bio-LSI without the light shield. This introduces significant advantages to biological measurements that are often performed under microscopic observation with lighting. The improved circuit realizes the mode selectable function that enables the individual operation of 400 electrodes in off, electrometer, V1, and V2 mode. The off-mode cut the electrode from the electric circuit. The electrometer-mode read out the electrode potential. The V1-mode and the V2-mode set the selected sensor electrode at two different independent voltages and read out the current generated on the surface of the electrode. This 4-mode selectable function of 2G Bio-LSI allows complex measurements and operations such as simultaneous detection of two different electrochemical active species, and selective modification of the electrodes for simultaneously detection of a number of items. We show some demonstrations in this paper to confirm the availability of these applications. We consider that the 4-mode selectable function are also applicable to highly sensitive

electrochemical measurements based of the redox cycling, imaging of the transients of the extracellular potential of the neuronal networks with electric stimulus, and manipulations of cells and particles using dielectrophoresis. As shown in these examples, the mode selectable function greatly extends the application range of Bio-LSI.

This study shows the effectiveness of LSI for electrochemical measurements at many sensing points. The results reveal that Bio-LSI is a widely applicable platform for bioimaging and biosensing, particularly for measurements requiring high sensitivity and complex operations.

2. Materials and methods

2.1. LSI circuit design architecture

The LSI chip was designed by Toppan Technical Design Center Co., Ltd. (Japan) using a 0.18-μm-ruled six-layer metal CMOS process for analog circuits. The chip was implemented at Semiconductor Manufacturing International Corporation (SMIC, China) on an 8-inch wafer. The fundamental design of the LSI circuit is the same as that of the previously reported 1G Bio-LSI.[10] Briefly, the LSI chip consists of a 20 × 20 array of analog pixel circuits (unit cells) and peripheral circuits, including a digital signal

controller to decode a column-selecting signal for the data output. Each unit cell has a switched capacitor I-V converter with an operational amplifier (op-amp) to detect very small currents generated on the sensor electrode with a high signal-to-noise ratio. The 2G Bio-LSI has a light shield consisting of a top metal layer of the LSI chip to prevent noise from the photocurrent. This top metal layer made of aluminum (1 μm in thickness) is a part of LSI structure (that is 6^{th} metal layer of six metal-oxide layered structure) incorporated into LSI chip on a metal deposition process at the LSI fabrication foundry. The light shield is designed to cover the metal-oxide-semiconductor (MOS) structures of the LSI circuit, except for metal-insulator-metal (MIM) structured parts on which a parasitic capacitance is potentially generated with the facing metal layer (Figure 2A). Figure 2B and 2C show comparative micrographs of a unit cell of 1G and 2G Bio-LSI chip before surface modification described in section 2.2, respectively. The area exhibiting uniformly orange tone in Figure 2C is covered with the light shield. As shown in these micrographs, the MOS elements visible in 1G Bio-LSI chip (Figure 2B) are hidden under the light shield for 2G Bio-LSI chip (Figure 2C). Switches for four-mode selection were added between the sensor pad and the switched capacitor for the I-V convertor in each unit cell (SW1–4 in Figure 3). A switch for resetting the switched capacitor (SW5) and a switch for readout the voltage from the op-amp (SW6)

were designed as for 1G Bio-LSI.

The selection of the mode of an individual unit cell is accomplished with SW1–4, as shown in Figure 3B. In the off-mode cells, the sensor electrodes are in an open circuit that is cut from the electrical circuit. On the electrometer-mode cells, the sensor electrodes are connected to the plus terminal of the op-amp to readout the voltage of the sensor electrode using the op-amp. The V1 and V2 modes are the potentiostat modes that enable us to set desired sensor electrodes at two different independent voltages for potential-controlled current measurements including cyclic voltammetry and chronoamperometry. In the V1 mode, the potential of the sensor electrodes are set V_1 V *vs.* reference electrode by controlling the potential of the reference electrode at $-V_1$ V *vs.* the ground potential through the counter electrode with a potentiostat circuit, under the condition that the plus and minus terminals of the op-amp are connected to the ground and the sensor electrode, respectively. Note that a pair of a reference electrode and a counter electrode is inserted into the solution on the sensor chip during the measurements. Because the potential of the sensor electrode is 0 V *vs.* the ground potential under this condition, the relative potential of the sensor is set at V_1 V *vs.* reference electrode. In the V2 mode, $(V_2 - V_1)$ V *vs.* the ground potential is applied to the plus terminal of the op-amp via the D/A converter by applying $-V_1$ *vs.* ground

potential to the reference electrode. As a result, the potential of the sensor electrode is set at V_2 V *vs.* the reference electrode. The operation of each of the 400 electrodes is easily programed by selecting each electrode mode from the four modes (Figure 3C).

Some incidental changes that are present in the proposed 2G Bio-LSI circuit are as follows. We added a row decoder to control the switches to select the mode of each unit cell. The power supply and signal control are realized with 50 pins. To incorporate additional circuits into the 250-μm-pitched unit cells, we reduced the size of the Al pads in the sensor area from 61.0 μm × 71.0 μm to 30.0 μm × 30.0 μm (Figure 2B, C) and the capacitance of the switched capacitors from 8 pF to 6 pF. The reduction in the sensor pad size made it impossible for the foundry to open contact holes; therefore, we opened contact holes using reactive ion etching (RIE).

2.2. LSI surface modification and LSI chip mounting on control system

The process of surface modification on the LSI chip to make sensor electrodes with noble metals and the procedure of LSI chip mounting on the substrate were identical to previously described methods;[10] however, the RIE process was added to open contact holes (indicated "a" in Figure 1D) for the sensor area in order to connect the sensor electrodes to the electric circuit under insulation layers on the surface of the LSI chip.

RIE was carried out using L-201D-L (Anelva Corp., Japan) with CHF_3 (20 sccm)/Ar (20 sccm) gas mixtures (5 Pa) at an RF power of 60 W to etch the SiO_2 and SiN layer on the Al pads, after the patterning of a positive photoresist (OFPR-800LB-200cp, Tokyo Ohka Kogyo Co., Ltd., Japan) onto a diced LSI chip (25 mm × 25 mm squares). After the removal of the photoresists with acetone (lift-off), we proceeded to fabricate the electrode structures and mount the LSI chip using the previously described methods.[10] Briefly, metals (Ti/Pt or Ti/Pt/Au) were deposited by sputtering (L-332S-FH; Anelva Corp., Japan) onto the open-holed LSI chip with the a positive photoresist bilayer pattern (OFPR-800LB-200cp, Tokyo Ohka Kogyo Co., Ltd., Japan; LOR 15A, MicroChem Corp., USA). After lift-off using acetone and a 502-A stripper (Tokyo Ohka Kogyo Co., Ltd., Japan), an insulation layer (~4-μm thick) was fabricated using a negative photoresist (SU-8 3005, MicroChem Corp., USA) to define the electrode area into a 40-μm diameter. The circle indicated as "b" in Figure 1D is the fabricated microelectrode. The surface-modified LSI chip was diced into a 10.4-mm square using a dicing machine (DAD522; Disco, Japan) and then glued onto a Au-wire patterned ceramic substrate with silver paste. The I/O pads of the LSI chip and the Au wire on the substrate were electrically connected using gold wires (25 μm in diameter) with a wire bonder (HB16; TPT Wire Bonder GmbH & Co. KG, Germany). After attaching a

polycarbonate resin wall to the ceramic substrate as a solution reservoir, the conductive wires inside the wall were covered with polydimethylsiloxane (PDMS). The appearance of the completed Bio-LSI chip is shown in Figure 1A.

2.3. Electrochemical measurements

The measurement system of 2G Bio-LSI is basically the same as that for 1G Bio-LSI; however, some circuits were added to the external circuit box to perform a 2G-specific operation. The system comprised an external circuit box with a pin connector to install the LSI chip unit, a DC power source box, a control unit (NI PXI-1031, NI PXI-8106, and NI PXI-6255, National Instruments Corporation, TX, USA), a monitor, and a keyboard. After the sample solution was installed into the polycarbonate wall on the Bio-LSI chip unit, a counter electrode and an Ag/AgCl reference electrode were inserted into the solution. As described in the previous paper,[10] we used an oxygen plasma generator (LTA-101, Yanaco Co., Japan) or carried out vacuum degassing before the solution was introduced into the electrode area, which was surrounded by the hydrophobic SU-8 resin. The measurements were performed using a program written in LabView ver. 2010 (National Instruments Corporation, TX, USA).

3. Results and discussion

3.1. Light-shielding effect of the metal layer of the LSI chip

We estimated the light-shielding effect of the top-metal layer of the 2G Bio-LSI by comparing the photocurrent generated on the 2G Bio-LSI chip to that on the 1G Bio-LSI chip lacking a light shield on the top metal (Figure 2B). This experiment was performed using the same procedure as that previously reported for 1G Bio-LSI with respect to the light-shielding effect of the sputtered Au layer.[10] The LSI chip mounted on the measurement system was irradiated with light using a stereoscopic microscope (S8APO, Leica Microsystems, IL, USA) with four different light intensities (inset of Figure 4A). The light intensities on the LSI chip were measured by an illuminometer (TMS201, Tasco, Japan). Both the room light and the microscope light were all-round white lights. The measurements were performed in the 0.1 nA range mode of the Bio-LSI measurement system. Figure 4 shows the results of the measured current generated by various light intensities (Figure 4A) with the magnified graph showing small currents (Figure 4B). The current increased linearly with the light intensity on the LSI surface in the range from 160 lx to 35,000 lx. This indicates that the current was the photocurrent generated on the diodes composed of LSI. With the 2G Bio-LSI chip, the photocurrent was suppressed to less than 1/100 by the light shield created by the top

metal layer of the LSI chip. The efficiency of the light shield as calculated by the photocurrent was 99% whereas that of the Au sputtering layer was 75%, according to the previous result.[10] The undesired influence of the photocurrent can be decreased from 90 pA to less than 1 pA (c.f. 22 pA using the Au sputtering layer in the previous report[10]) even under optical observation with a microscope under the most intense lighting condition (35000 lx). This introduces significant advantages to biological measurements that are often performed under microscopic observation with lighting.

3.2. Demonstration of the mode-selectable function (V1 and V2 modes) for redox measurement

To demonstrate the mode-selectable function, we displayed a dot picture using the 2G Bio-LSI chip with 400 Au electrodes (each 40 μm in diameter) based on the redox reaction of $FcCH_2OH$ using the V1 and V2 modes. We stepped the potential of the electrodes composing characters of "Bio LSI 2G" (shown in blue in Figure 5A) from 0.0 V to 0.5 V *vs.* Ag/AgCl using the V2 mode, whereas the other electrodes (shown in red in Figure 5A) were maintained at 0.0 V *vs.* Ag/AgCl using the V1 mode. The series of images based on the redox reaction after the potential step is shown in Figure 5B. In the image of 1s after the potential step, the oxidation current of $FcCH_2OH$ was observed

at the measurement points composing characters with an applied voltage of 0.5 V vs. Ag/AgCl, whereas almost no current was observed at the remained measurement points with an applied voltage of 0.0 V vs. Ag/AgCl, resulting in the display of the characters of "Bio LSI 2G." In the images of more than 50 s passed from the time of the potential step, the expanding black areas with reduction currents are observed around the characters. This indicates that the diffusion and the reduction of the $Fc^{+}CH_2OH$ generated by the oxidation of $FcCH_2OH$ at the measurement points composing characters diffused onto the surrounding electrodes were set to 0.0 V to give a reduction current. These results indicate the suitability of the V1 and V2 modes of 2G Bio-LSI.

3.3. Demonstration of the mode-selectable function (V1 and V2 modes) for the simultaneous detection of O_2 and H_2O_2

We then used the V1 and V2 modes for the simultaneous detection of O_2 and H_2O_2 on a single Bio-LSI chip with 400 Pt electrodes (each 40 μm in diameter). We poured air-saturated phosphate buffered saline (PBS) into the polycarbonate reservoir of the Bio-LSI chip and then applied −0.5 V *vs.* Ag/AgCl to the electrodes on the left half of the sensor area for O_2 detection and 0.7 V *vs.* Ag/AgCl to the electrodes on the right half of the sensor area for H_2O_2 detection (Figure 6A). After the currents reached steady

state, we injected 0.5 mM H_2O_2 from the right-hand side of the sensor chip using a microsyringe pump (BS-MD 1001; BAS Bioanalytical Systems Inc., USA) through a fused silica capillary tube (ID = 120 μm, OD = 250 μm; GL science, Japan) at 50 μL/min (Figure 6B-a). After 30 s from the start of H_2O_2 injection, we started to inject 0.1 M Na_2SO_3 at 2 μL/min from the left-hand side of the sensor chip (Figure 6B-b). Na_2SO_3 reduces oxygen to decrease the concentration of dissolved oxygen. Figure 6C shows the changes in the monitored current after the H_2O_2 injection and subsequent Na_2SO_3 injection. Before the H_2O_2 injection, reduction currents were observed at the electrodes on the left-hand side, whereas almost no currents were observed at the electrodes on the right-hand side. These reduction currents were derived from the reduction of dissolved oxygen at -0.5 V *vs.* Ag/AgCl. After the injection of H_2O_2, the increases in the oxidation currents were observed on the right-hand side with an applied potential of 0.7 V *vs.* Ag/AgCl, because the injected H_2O_2 was oxidized at 0.7 V *vs.* Ag/AgCl. After the injection of Na_2SO_3, we observed decreases in the reduction currents on the left-hand side with an applied potential of -0.5 V *vs.* Ag/AgCl. The decrease in the reduction currents indicates a decrease in the concentration of O_2 due to the injection of Na_2SO_3. When Na_2SO_3 reached the right-hand side, the oxidation

currents on the electrodes on the right-hand side increased owing to the oxidation of Na_2SO_3 at 0.7 V vs. Ag/AgCl.

3.4. Demonstration of the mode-selectable function (off and V1 modes) for selective modification of electrodes

We also demonstrated the mode-selectable function of 2G Bio-LSI, which enables the selective modification of the 400 electrodes. We employed a commercially available osmium-polyvinylpyridine gel polymer containing horseradish peroxidase (Os-HRP; BAS Inc., USA) as a surface modifier for the selected electrodes. Os-HRP, which was invented by Heller *et al.*,[14] has been used for various biosensor elements[15] because of its high sensitivity for the electrochemical detection of H_2O_2 at a lower operational potential. The osmium-polyvinylpyridine gel polymer can be electrodeposited onto the electrode by cycling the electrode potential with co-electrodeposition of the HRP.[16] We placed 80 μL of two-times diluted Os-HRP with PBS in the polycarbonate reservoir on the Bio-LSI chip. After inserting an Ag/AgCl reference electrode and a Pt counter electrode, we scanned the potential of the selected electrodes (V1 mode) from 1.0 V to -0.4 V *vs.* Ag/AgCl for 25 or 50 cycles at 100 mV/s. The other electrodes remained in the off mode. Figure 7A shows photographs of the unit cells on a chip after the selected

electrodeposition of Os-HRP. The color of the V1-mode electrodes changed to brown by the deposition of HRP molecules. Compared to the 25-cycle electrodes, the 50-cycle electrodes exhibited a darker color because of the deposition of a large amount of Os-HRP.

We estimated the amount of the deposited Os using cyclic voltammetry. Figure 7B shows typical cyclic voltammograms obtained by the Os-HRP-deposited 2G Bio-LSI chip in the PBS solution. The cyclic voltammograms exhibited almost symmetric oxidation and reduction waves around the potential of 0.33 V. The shapes were consistent with those reported in previous papers.[14,15f] This shape is typical for surface-confined redox species. The surface concentrations of the redox site (Os molecules) calculated from a coulometric analysis of the peaks were 1.0 nmol/cm^2 and 1.2 nmol/cm^2 for 25-cycle and 50-cycle electrodes, respectively. Compared to the voltammogram of the 25-cycle electrode, the voltammogram of the 50-cycle electrodes exhibited a smaller axial symmetric property with a diffusion tail like form. We consider that the Os-HRP layer of the 50-cycle electrode was thick, with more than 1.2 nmol/cm^2 of Os molecules at the outer layer, from which electrons hopped onto the surface of the electrode, resulting in the formation of the diffusion tail of the

voltammetric curve. The electrodes selected in the off mode exhibited a small peak (ca 20 nA) by the nonspecific adsorption of Os onto the electrode.

Next, we demonstrated H_2O_2 detection using the Os-HRP-deposited 2G Bio-LSI chip. The potential of the 400 electrodes was maintained at 0.0 V to detect the reduction of Os^{3+} generated by HRP-catalyzed H_2O_2 oxidation. Figure 7C shows the typical chronoamperometric responses for the successive addition of 20 μL of 1.0 mM H_2O_2 to 2 mL of PBS in the wall of the 2G Bio-LSI chip. The interval between subsequent additions of H_2O_2 was 100 s with 3 s of vigorous pipetting to mix the solution. For each addition of H_2O_2, the reduction current immediately increased and then reached a steady state. The response current at steady state increased with the concentration of H_2O_2 in the solution (Figure 7D). The average current monitored for the 50-cycle electrodes was 1.3 times higher than that monitored for the 25-cycle electrodes. This is a reasonable result based on the cyclic voltammograms in Figure 7B, in which the reduction peak current of the 50-cycle electrodes was observed to be 1.3 times higher than that of the 25-cycle electrodes. No significant current increase was observed for the non-cycled electrodes. These results indicate that we successfully modified the selected electrodes with Os-HRP using the off and V1 modes. This technology is usable for various

applications of electrode modification using electrodeposition for simultaneous multianalysis.

4. Conclusion

In this study, we developed an advanced version of Bio-LSI called "2G Bio-LSI." The basic LSI circuit design and architecture of 2G Bio-LSI were similar to those of the previously developed Bio-LSI with an 400-amperometric sensor array fabricated by a 0.18-μm-ruled six-layer metal CMOS process for analog circuits. Advanced points of the 2G Bio-LSI are an effective removal of photocurrent noise and an improvement of control/measurement circuit to allow individual operation of 400 electrodes. The light shield created by the top metal layer of the LSI chip effectively reduced the photocurrent resulting in a reduction in the undesired noise current due to light irradiation to less than 1 pA, even under optical observation with a microscope using the most intense lighting (35000 lx). This introduces significant advantages to biological imaging that are often obtained under microscopic observation with lighting. The 400 sensing points exhibited good agreement with the theoretically predicted voltammetric behavior. 2G Bio-LSI may also be used as a very reliable electrometer array. Using the mode-selectable function, we displayed a dot picture based on the

redox reaction of 2.0 mM $FcCH_2OH$ using the V1 and V2 modes. We also carried out the simultaneous detection of O_2 and H_2O_2 on one chip using the V1 and V2 modes by applying -0.5 V and 0.7 V *vs.* Ag/AgCl to the electrodes for O_2 and H_2O_2 detection, respectively. The mode-selectable function enabled the modification of selected electrodes with Os-HRP using the off and V1 modes. The Os-HRP-deposited electrodes exhibited obvious chronoamperometric responses to the successive addition of H_2O_2 up to 10 μM (final concentration), whereas the non-deposited electrodes did not exhibit any significant responses. These successful results strongly indicate that 2G Bio-LSI is a promising tool for a wide range of analytical fields. Currently, we are in the process of developing multiple applications of 2G Bio-LSI, the integration of boron-doped diamond electrodes[17] and the integration of conductive amorphous carbon nitride electrodes[18] as well as improving the time resolution of Bio-LSI. These efforts will further expand the usefulness of Bio-LSI as a rapid and high-throughput quantitative analysis platform for biomolecules and bioimaging based on amperometric detection.

Acknowledgements

This research was supported by Special Coordination Funds for Promoting Science and Technology, Creation of Innovation Centers for Advanced Interdisciplinary

Research Areas Program from the Japan Science and Technology Agency and was partially supported by a Grant-in-Aid for Scientific Research (A) (No. 22245011) and a Grant-in-Aid for Scientific Research (A) (No. 25248032) from the Japan Society for the Promotion of Science (JSPS).

References

1. S. Y. Joo and R. B. Brown, *Chem. Rev.*, 2008, **108**, 638-651.

2. T. Sakata and Y. Miyahara, *ChemBioChem* 2005, **6**, 703-710.

3. L. Berdondini, K. Imfeld, A. Maccione, M. Tedesco, S. Neukom, M. Koudelka-Hep and S. Martinoia, *Lab. Chip*, 2009, **9**, 2644–2651.

4. J. Rothe, M. K. Lewandowska, F. Heer, O. Frey and A. Hierlemann, *J. Micromech. Microeng.*, 2011, **21**, 054010

5. A. L. Ghindilis, M. W. Smith, K. R. Schwarzkopf, K. M. Roth, K. Peyvan, S. B. Munro, M. J. Lodes, Axel G. Stöver, K. Bernards, K. Dill and A. McShea, *Biosens. Bioelectron.*, 2007, **22**, 1853–1860.

6. M. Schienle, C. Paulus, A. Frey, F. Hofmann, B. Holzapfl, P. Schindler-Bauer and R. Thewes, *IEEE J. Solid-State Circuits*, 2004, **39**, 2438–2445.

7. P. Kruppa, A. Frey, I. Kuehne, M. Schienle, N. Persike, T. Kratzmueller, G. Hartwich and D. Schmitt-Landsiedel, *Biosens. Bioelectron*. 2010, **26**, 1414–1419.

8. B. N. Kim, A. D. Herbst, S. J. Kim, B. A. Minch and M. Lindau., *Biosens. Bioelectron.*, 2013, **41**, 736–744.

9. B. Lim, M. Futagawa, S. Takahashi, F. Dasai, M. Ishida and K. Sawada, *Jpn. J. Appl. Phys.*, 2014, **53**, 0465021-0465025.

10. K. Y. Inoue, M. Matsudaira, R. Kubo, M. Nakano, S. Yoshida, S. Matsuzaki, A. Suda, R. Kunikata, T. Kimura, R. Tsurumi, T. Shioya, K. Ino, H. Shiku, S. Satoh, M. Esashi and T. Matsue, *Lab Chip*, 2012, **12**, 3481–3490.

11. T. Hokuto, T. Yasukawa, R. Kunikata, A. Suda, K. Y. Inoue, T. Matsue and F. Mizutani, *Chem. Lett.*, 2013, **43**, 758–759.

12. M. Şen, K. Ino, K. Y. Inoue, T. Arai, T. Nishijo, A. Suda, R. Kunikata, H. Shiku and T. Matsue, *Biosens. Bioelectron.*, 2013, **48**, 12–18.

13. M. Şen, K. Ino, K. Y. Inoue, A. Suda, R. Kunikata, M. Matsudaira, H. Shikua and T. Matsue, *Anal. Methods*, 2014, **6**, 6337–6342.

14. M. Vreeke, R.Maidan and A. Heller, *Anal. Chem.*, 1992, **64**, 3084–3090.

15. a) M. G. Garguilo and A. C. Michael, *Anal. Chem.*, 1994, **66**, 2621–2629. b) N. Kasai, C. X. Han and K. Torimitsu, *Sens. Actuators B Chem.*, 2005, **108**, 746–750. c) H. Matsuura, Y. Sato, O. Niwa and F. Mizutani, *Anal. Chem.*, 2005, **77**, 4235–4240. d) F. Mizutani, E. Ohta, Y. Mie, O. Niwa and T. Yasukawa, *Sens. Actuators B Chem.*, 20008, **135**, 304–308. e) K. Nakajima, T. Yamagiwa, A. Hirano and M. Sugawara, *Anal. Sci.*, 2003, **19**, 55–60. f) K. Y. Inoue, K. Ino, H. Shiku, S. Kasai, T. Yasukawa, F. Mizutani and T. Matsue, *Biosens. Bioelectron.*, 2010, **25**, 1723–1728.

16. Z. Q. Gao, G. Binyamin, H. H. Kim, S. C. Barton, Y. C. Zhang and A. Heller, *Angew.*

Chem. Int. Ed. **41**, 2002, 810–813.

17. T. Hayasaka, S. Yoshida, K. Y. Inoue, M. Nakano, T. Ishikawa, T. Matsue, M. Esashi and S.Tanaka, *Technical Digest IEEE MEMS 2014, San Francisco, USA (2014, Jan.26 –30)*, 2014, 322–325.

18. Y. Kikuchi, A. Wada, T. Kurotori, M. Nakano, K. Y. Inoue, T. Matsue, T. Nozawa, and S. Samukawa, *Carbon*, **67**, 2014, 635–642.

FIGURE CAPTIONS

Figure 1 (A) Photograph of a Bio-LSI chip mounted on the ceramic substrate with a polycarbonate resin wall. (B) Magnification of an LSI chip part. (C) Micrograph of part of an electrode array. (D) Micrograph of a unit cell with an Al pad (a) and a sensing point (b).

Figure 2 (A) Schematic illustration of the cross section of a unit cell showing the light-shielding structure of the top metal layer of the LSI chip. (B) Micrograph of a unit cell of 1G Bio-LSI. (C) Micrograph of a unit cell of 2G Bio-LSI.

Figure 3 (A) Circuit diagram of a unit cell of 2G Bio-LSI. (B) Switch status of the four modes of 2G Bio-LSI (a–d) compared to the 1G Bio-LSI circuit (e). (C) An example of the mode setting screen of the 400 electrodes.

Figure 4 (A) Amperograms obtained by light exposure to 1G Bio-LSI (red line) and 2G Bio-LSI (blue line). The intensities of the light and the light sources are as follows: (a) 0 lx in a dark room, (b) 160 lx with room light, (c) 35000 lx with high-intensity microscope light, (d) 22000 lx with microscope light in the higher-middle intensity

range, (e) 11000 lx with microscope light in the lower-middle intensity range, (f) 3000 lx with the low-intensity microscope light. The inset shows the experimental settings. (B) Magnified graph showing the small current.

Figure 5 (A) Configuration of the mode of the 400 electrodes used in the demonstration to show a dot picture. (B) Color maps indicating the current intensities of 400 electrodes in the configuration of Figure A. The time-dependent transient of the maps after the potential step of the V2-mode electrodes is shown in six images.

Figure ~~6~~ (A) Configuration of the mode of the 400 electrodes to demonstrate the simultaneous detection of O_2 and H_2O_2. (B) Illustration showing the experimental setup of the demonstration. (C) The time-dependent transient of the color maps indicating the current intensities of 400 electrodes after the injection of H_2O_2 solution.

Figure ~~7~~ (A) Photographs of the unit cells in a 2G Bio-LSI chip after the selective electrodeposition of Os-HRP. (B) Typical cyclic voltammograms obtained by the Os-HRP-deposited 2G Bio-LSI chip in the PBS solution. (C) Typical chronoamperometric responses for the successive addition of 20 μL of 1.0 mM H_2O_2 into 2 mL of PBS in the polycarbonate resin wall of 2G Bio-LSI. The applied voltage

was 0.0 V *vs.* Ag/AgCl. (D) The plot of the steady-state current versus the final concentration of injected H_2O_2. Each plot and error bar represented the average and standard deviation of the currents, respectively, which were obtained with multiple electrodes on a chip.

Figure 1

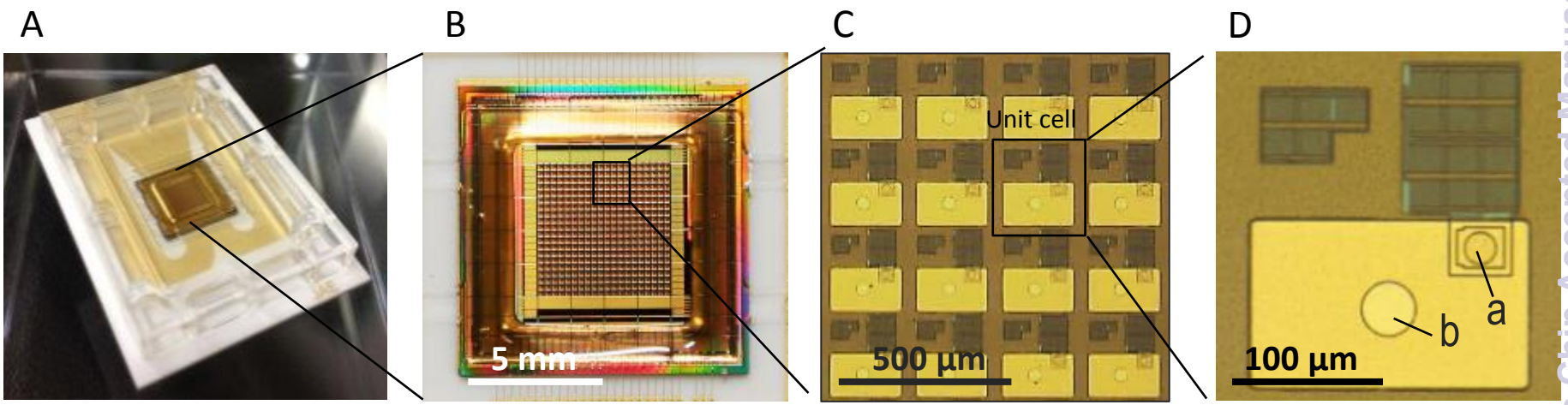

Figure 2

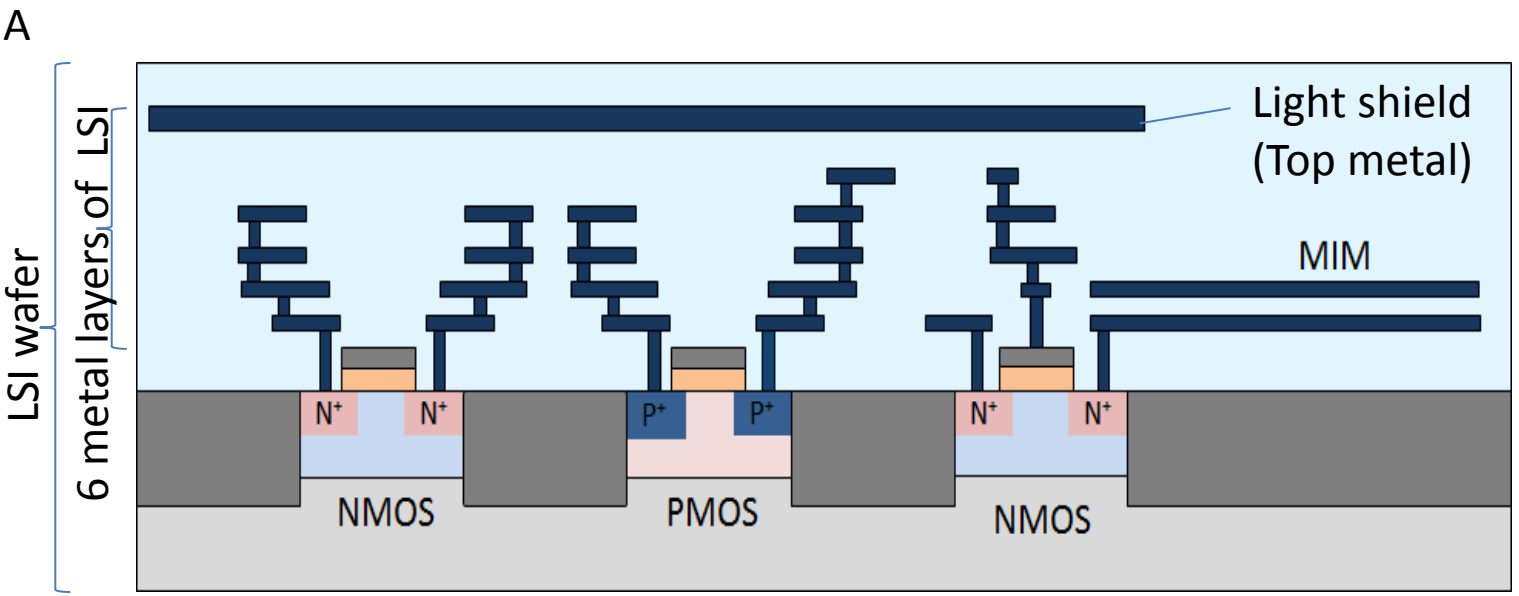

Figure 3

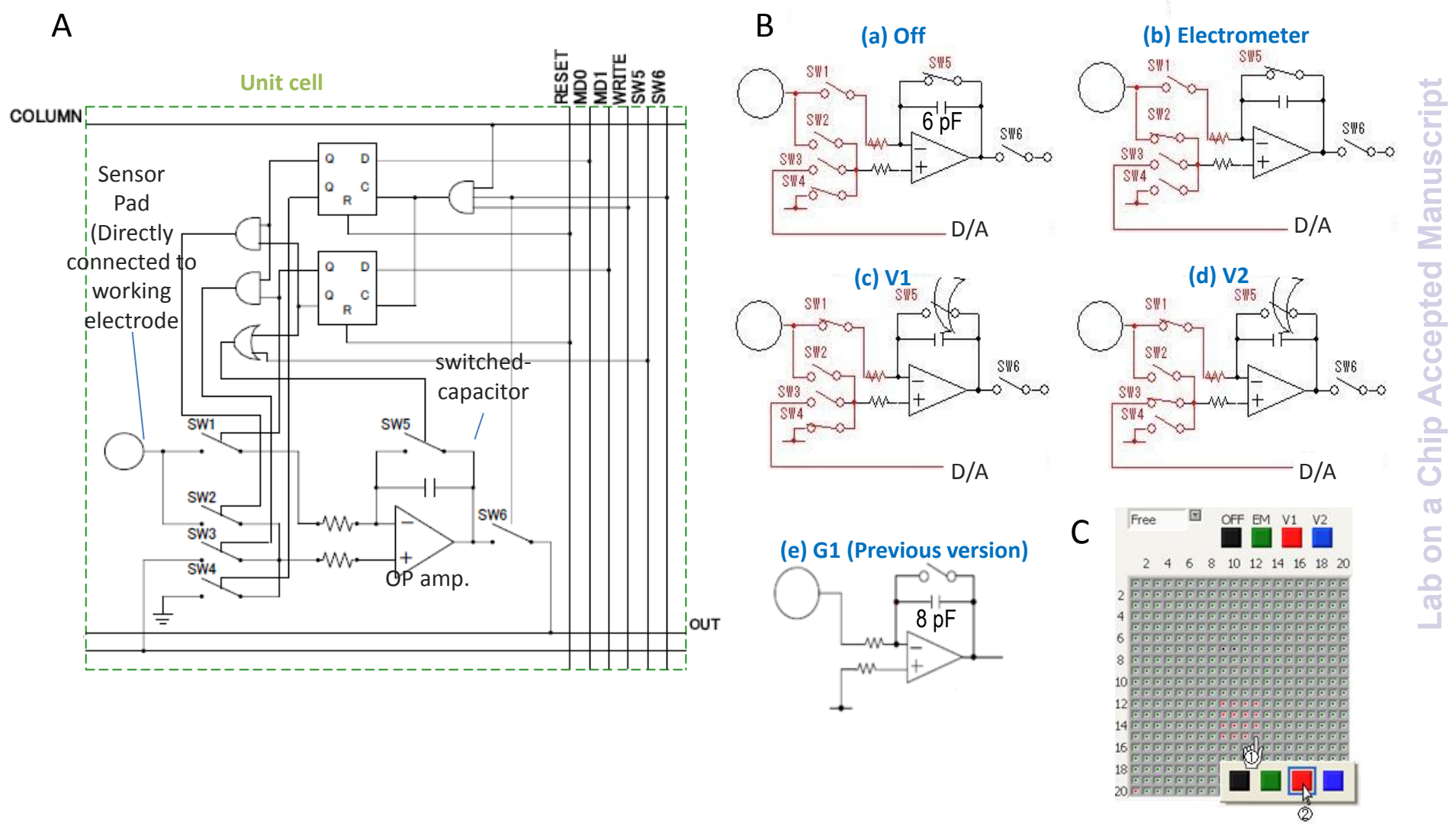

Figure 4

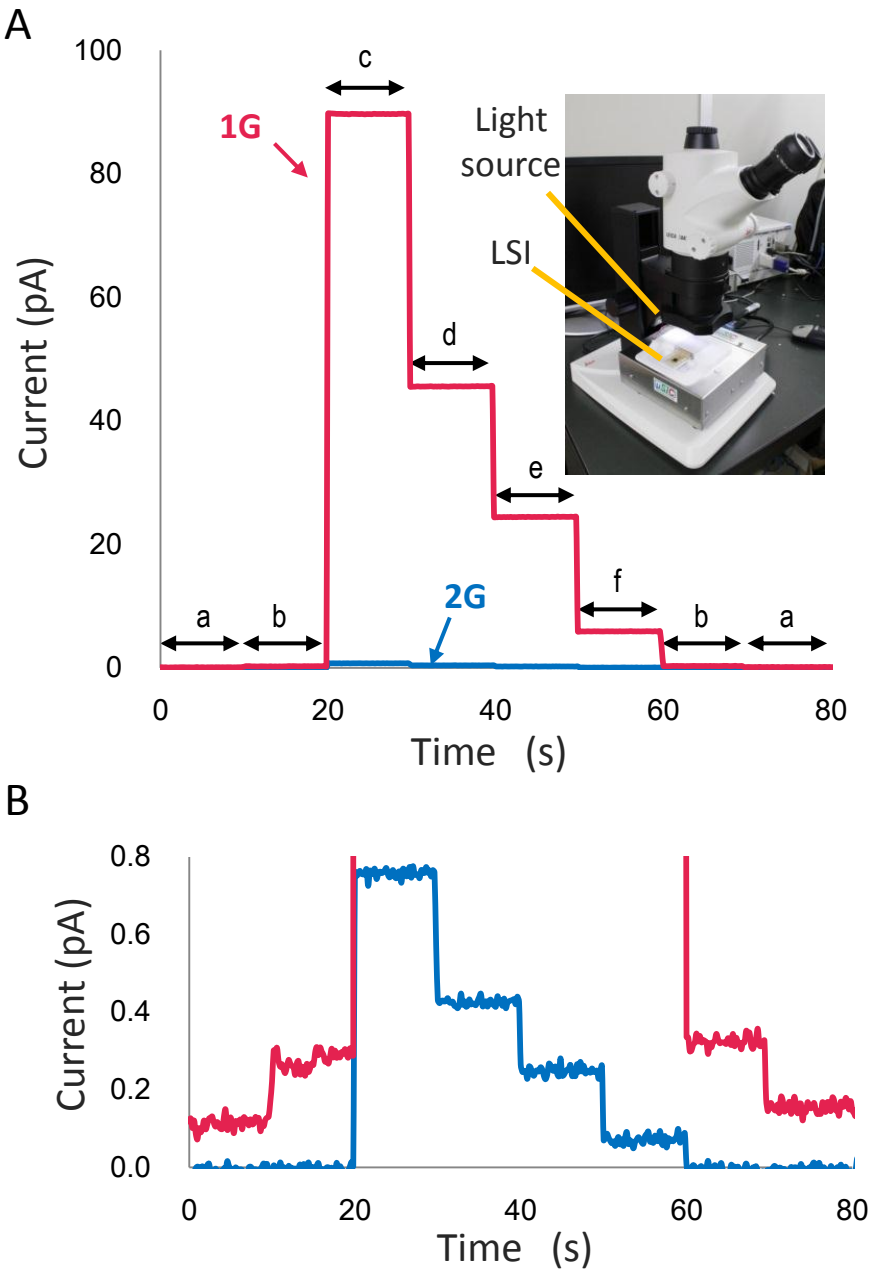

Figure 5

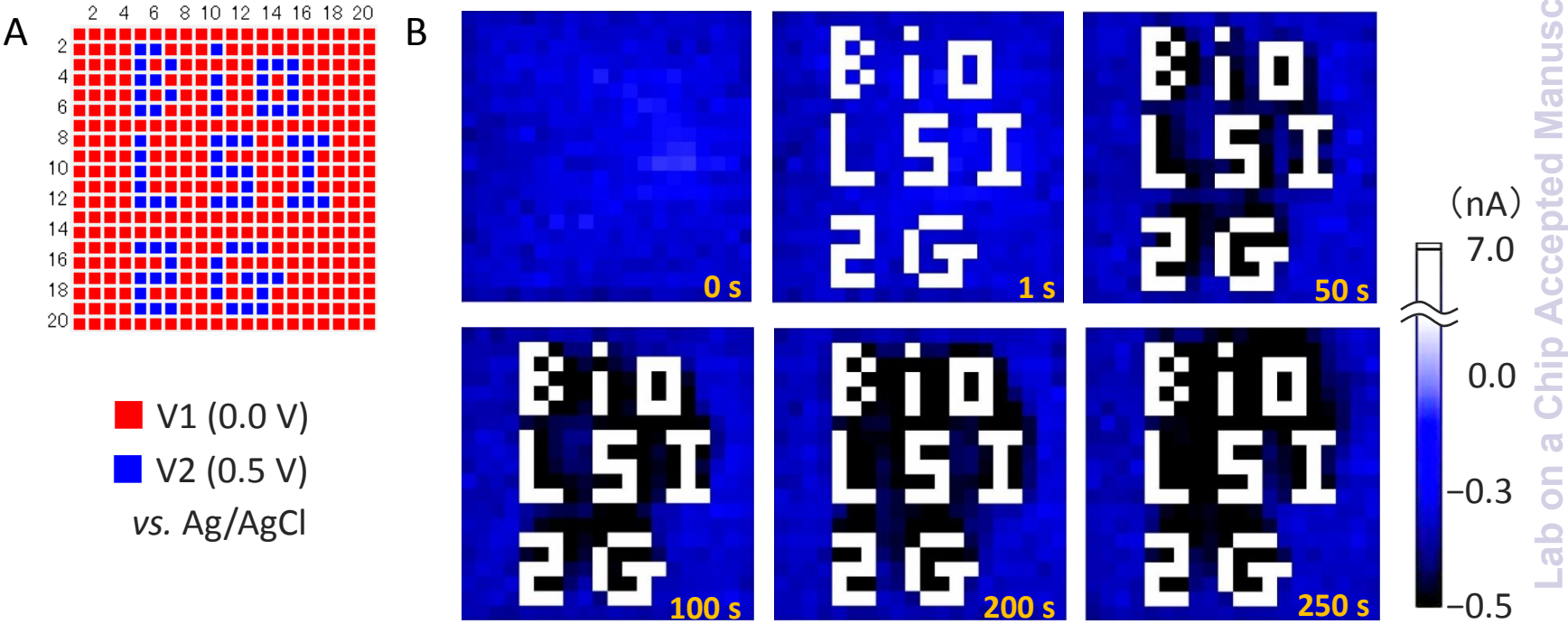

Figure 6

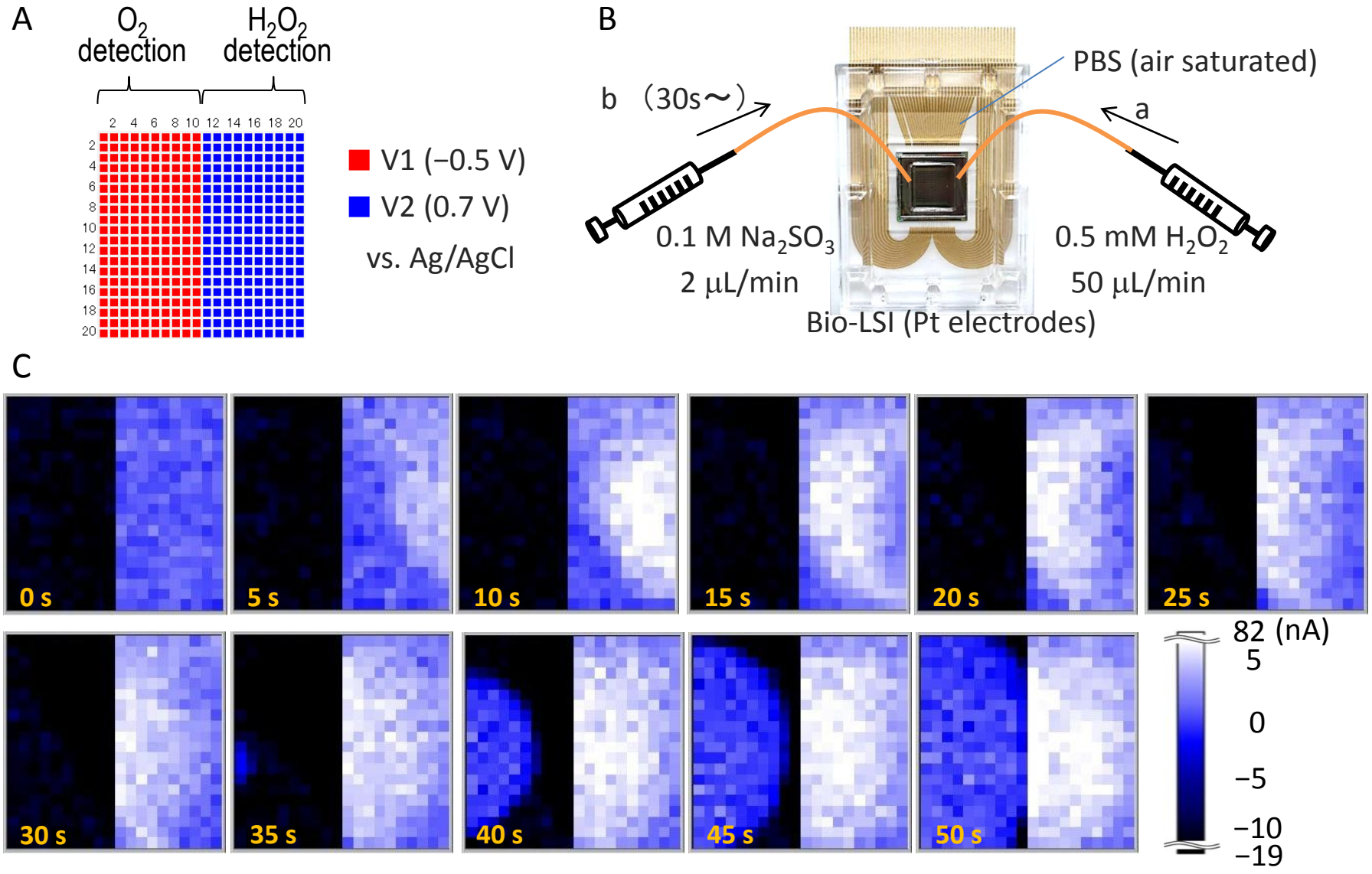

Figure 7

A

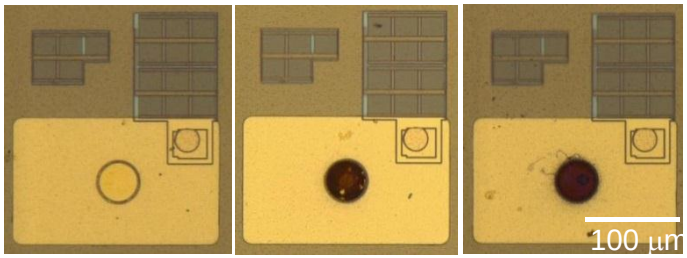

B

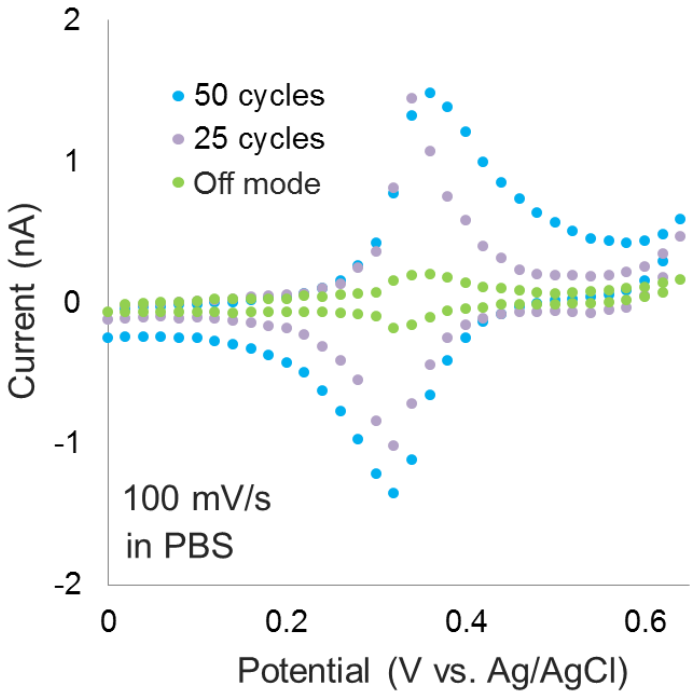

Figure 7

(Continued)

C

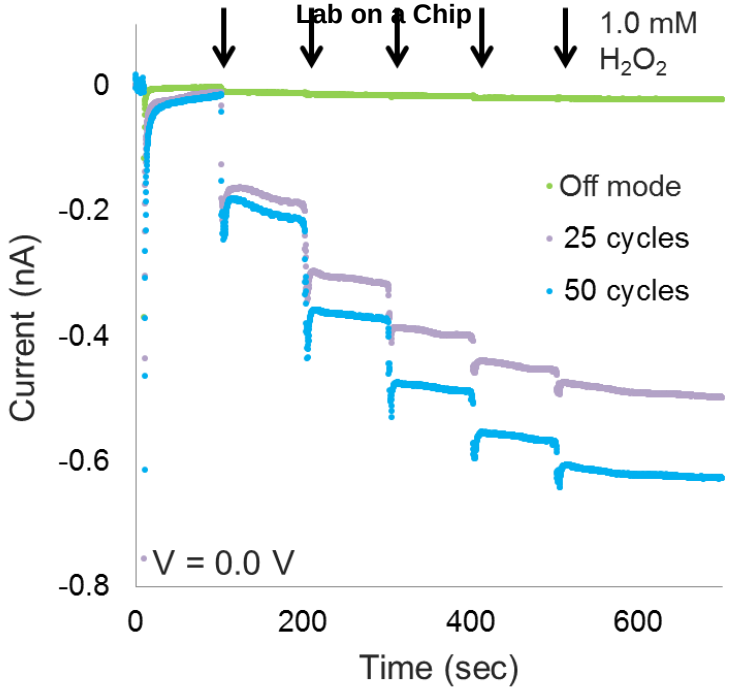

D